International Journal of Control and Automation
Vol.6, No.6 (2013), pp.127-138
http://dx.doi.org/10.14257/ijca.2013.6.6.13

Numerical Simulation and Analysis of Three Dimensional Flow Field of a Counter-Rotating Fan with Various Angles

Jiabin Wen and Haibo He

(College of Electrical and Electronic Engineering Harbin University of Science and Technology Harbin 150080 China)

hjyjh2010@163.com,wenjiabin@126.com

Abstract

In this paper, a type of a mining counter-rotating fan (FBCDZNO14) was taken as an example, we built a three-dimensional model of a whole machine from the inlet of a collector to the outlet of a diffuser, and the whole flow field was performed a numerical simulation and steady flow calculation was completed, at the same time, the results of numerical simulation were analyzed. The numerical results were compared with the experimental results, they had the same trend, and the error was in the acceptable range. We changed the two impellers blade setting angles, and simulated the counter-rotating fan with different setting angles. Simulation results reveal that the setting angles have impacts on the fan's flow, pressure head and efficiency, and provide theoretical bases for improving the operating efficiency and energy-saving control, at the same time, lay the foundation for the counter-rotating fan's optimal design.

Keywords: *the counter-rotating fan; numerical simulation; setting angle; performance analysis*

1. Introduction

The counter-rotating fan is a local fan's replacement product in the mine; it is the development and production after digesting and absorbing the foreign new technologies in 1980s [1]. Looking from the overall structure, it is an electromechanical integration device with multistage aerodynamic force and multistage electromagnetic force interaction. It has high pressure coefficient, good anti- wind performance, high efficiency, compact structure, etc. In the mines, tunnels, shipping and other areas of ventilation, the counter-rotating fan obtains a wide range of applications [2-4].

The research on counter-rotating fan started relatively late in our country, from the 1990s onwards, in order to meet the needs of mine ventilation , a series of studies has been carried out to reduce flow losses, improve efficiency and reduce noise [5- 6]. At present, domestic and foreign research on counter-rotating fan focuses on two-level counter-rotating impellers region, people are not familiar with the complex three-dimensional turbulent flow and the distribution of airflow pressure pulsation inside the counter-rotating fan. However, along with the emergence of long-distance air conveying, the performance of the counter-rotating fan has become increasingly demanding [7]. Since the similarity theory does not apply, the traditional design methods strong depend on tests, using the test methods monitor the pressure pulsation inside the counter-rotating fan especially on the rotating impellers, but this method is more difficult, it needs to consume a lot of manpower and financial resources, and the development cycle is longer. The numerical simulation method links theoretical analysis and experimental

ISSN: 2005-4297 IJCA

study, with its unique advantages it is gradually becoming an important means of researching the fluid flow patterns, it can greatly reduce development time, costs and avoid the risks of new designs [8- 9].

In this paper, the 3D steady constant flow field is calculated by using the method of CFD in order to obtain the details of fluid flow, and analyze the counter-rotating fan's performance and characteristics based on the results of the numerical simulation.

2. The Model of Three Dimensional Global Fluid Field

2.1. Physical model

In order to make a comprehensive study of the counter-rotating fan's performance and features, we take a FBCDZNO14 mine counter-rotating fan as an example and establish two impeller models in accordance with the design drawings. The two impellers are made of twisted airfoil-shaped blades whose numbers are respectively 13 and 11. Two impellers rotate in opposite directions at the speed of 980r/min. Using pre-processing software Gambit to establish the whole model. Figure 1 shows the structure of the counter-rotating fan. Figure 2 shows the counter-rotating fan's global flow model.

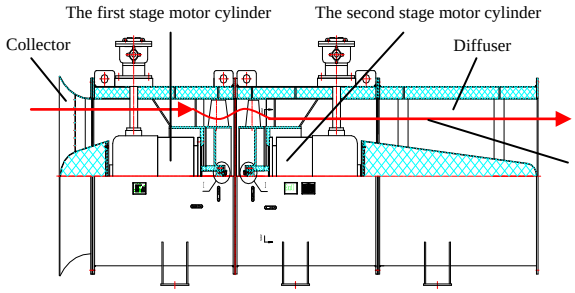

Figure 1. The structure of the counter-rotating fan

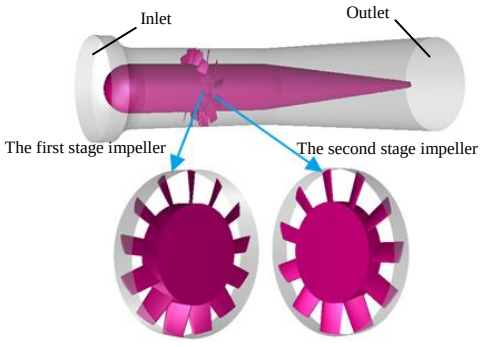

Figure 2. The global flow field model of the counter rotating fan

2.2. Mathematic model

The flow of fluid within counter-rotating fan follows the law of conservation of mass and momentum conservation law, and meets the quality continuity equation and Navier-Stokes equations. Meanwhile, the fluid flow is turbulent and viscous, so it needs comply with the additional turbulence transport equation. We ignore the heat exchange and the influence of

gravity during calculating the fluid flow, and assume the fluid is incompressible in a steady flow state.

Mass conservation equation:

$$\frac{\partial \rho}{\partial t} + \operatorname{div}(\rho \boldsymbol{u}) = 0 \tag{1}$$

Momentum conservation equation:

$$\left.\begin{aligned} \frac{\partial(\rho u)}{\partial t} + \operatorname{div}(\rho u \boldsymbol{u}) &= \operatorname{div}(\mu \operatorname{grad} u) - \frac{\partial p}{\partial x} + S_u \\ \frac{\partial(\rho v)}{\partial t} + \operatorname{div}(\rho v \boldsymbol{u}) &= \operatorname{div}(\mu \operatorname{grad} v) - \frac{\partial p}{\partial y} + S_v \\ \frac{\partial(\rho w)}{\partial t} + \operatorname{div}(\rho w \boldsymbol{u}) &= \operatorname{div}(\mu \operatorname{grad} w) - \frac{\partial p}{\partial z} + S_w \end{aligned}\right\} \tag{2}$$

Where $\boldsymbol{u}$ is the velocity vector; u、v、w are respectively represent velocity vector component in x、y、z directions; ρ is the density; μ is the dynamic viscosity; S_u、S_v、S_w are the generalized source terms of Navier-Stokes equations; p is the pressure on the micro fluid unit [10].

Turbulence model uses RNG k-ε two-equation model based on Reynolds averaging method, and the corresponding k and ε transport equations are:

$$\frac{\partial(\rho k)}{\partial t} + \frac{\partial(\rho k u_i)}{\partial x_i} = \frac{\partial}{\partial x_j}\left[\alpha_k \mu_{eff} \frac{\partial k}{\partial x_j}\right] + G_k + \rho\varepsilon \tag{3}$$

$$\frac{\partial(\rho \varepsilon)}{\partial t} + \frac{\partial(\rho \varepsilon u_i)}{\partial x_i} = \frac{\partial}{\partial x_j}\left[\alpha_\varepsilon \mu_{eff} \frac{\partial \varepsilon}{\partial x_j}\right] + \frac{G_{1\varepsilon}^* \varepsilon}{k} G_k - C_{2\varepsilon}\rho \frac{\varepsilon^2}{k} \tag{4}$$

Where k is turbulent kinetic energy; ε is dissipation rate of turbulent kinetic energy; G_k is a production term of turbulent energy k caused by the mean velocity gradient, $G_k = \mu_t\left(\frac{\partial u_i}{\partial x_j} + \frac{\partial u_j}{\partial x_i}\right)\frac{\partial u_i}{\partial x_j}$; μ_{eff} is equivalent viscosity coefficient [10].

2.3. Assumptions and numerical calculation

The basic assumptions of fluid flow within counter-rotating fan are given as following:

(1) The fluid Reynolds number is large (Re> 2300), it belongs to turbulence, so we use of turbulence model for solving fluid field.

(2) Ignore the buoyancy and gravity of the fluid at standard atmospheric pressure.

(3) Fluid flow rate is much less than the speed of sound that is the Mach number (Ma number) is small, so the fluid is considered as incompressible fluid.

(4) Since we only study the fluid flow's steady state, so the equations don't contain time items.

The global three-dimensional flow field within counter-rotating fan is divided by unstructured tetrahedral mesh, since the turbulence at the two impellers changes tempestuously, so the grid is dense here. Eventually the computational domain's grid cell number is 3352464, two impellers parts' grid cell number is 2057496.

According to the counter-rotating fan's structure and its internal fluid flow characteristics, the value of the boundary condition is given as follows: speed entry, free outlet, the mainstream flows along the axial direction. Define the region of the two impellers as rotation region; approach the multiple rotating coordinate systems MRF (moving reference frame) to deal with the two impellers' rotation [11-12].

Sliding mesh is used to achieve the information transfer between interfaces. Solve equations using separation implicit solver, select SIMPLE algorithm to achieve pressure-velocity coupling, use second-order upwind to build discrete equations. Fluid-solid contact surface is solid wall with no-slip conditions, and a standard wall function is used in the near wall region. We calculate the three-dimensional flow field domain model in different conditions within the counter-rotating fan's ventilation system by the method of finite volume.

4. Simulation Results and Analysis

4.1. Pressure field and velocity field analysis

The global three-dimensional flow field within the counter-rotating fan is calculated, and we get the distribution of the internal fluid pressure pulsation. Figure 3 shows the static pressure distribution in axial sections, in which (a), (b), (c) respectively represent the inlet section of the first stage impeller, middle section between two impellers and the exit section of the second impeller. The pressure field distribution along the axial direction can be seen substantially from figure. Static pressure distribution in the circumferential direction has good symmetry, this shows that when the counter-rotating fan operates at the design flow range, the internal flow field is relatively stable and turbulence is not obvious. The figure shows that the third section's static pressure increase significantly after the two impellers doing work, the static pressure in these sections change cyclically and alternately with good symmetry. The static pressure is slightly lower from the outside to the inside in the radial direction of figure.

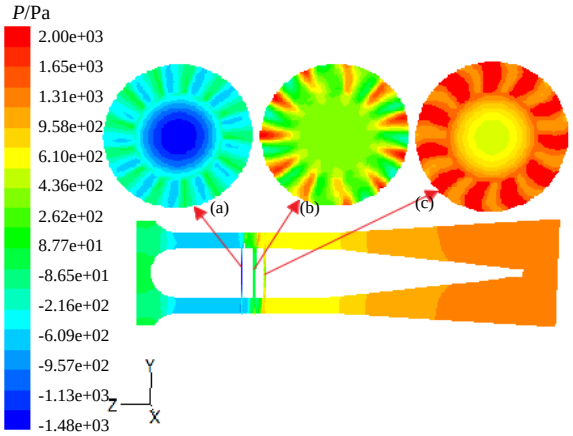

Figure 3. The static pressure distribution chart in axial section

Figure 4 shows the statistical distribution of the static pressure value on the node grid in the axial direction. Where wall represents the first impeller, wall: 001 represents the second impeller, wall 7 represents the internal wall of the fan. The counter-rotating fan's internal static pressure significantly increases after the first impeller doing work and static pressure rises to the top after the second impeller doing work, and then it gradually decreases. The fan can access to sufficient pressure rise in exit after diffusion of the diffuser.

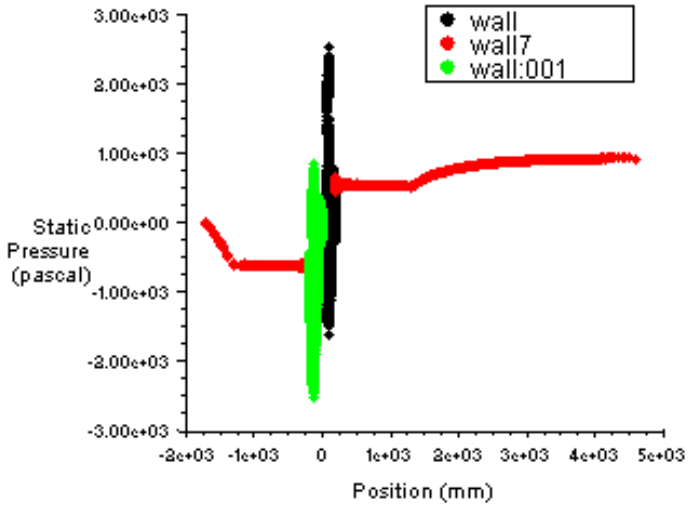

Figure 4. The statistical distribution of the static pressure value on the node grid in the axial direction

Figure 5 shows the static pressure distribution in two-level impellers' root segments and blades, in which (a), (b) respectively represent the first stage impeller and the second stage impeller. The two impellers are main parts doing work in the counter-rotating fan. The static pressure in their surface changes drastically, there isn't banded distribution like a collector an*d a diffuser*. The figure shows that the value of static pressure near the pressure side is greater than it near the suction side, so there is a large pressure difference in the front and rear sides of the blade root, this will result in a greater perturbation and a high degree of turbulence. In addition, static pressure in the first stage impeller's root is lower than it in the second stage impeller's root, the pressure distribution in the impellers' surface has good symmetry in the circumferential direction. The impellers' pressure surface pushes air flow to do work, the static pressure in pressure surface is positive, and there is a negative pressure zone in suction surface, so the static pressure in it is negative. Since the fluid first collide with the leading edge of the pressure surface, therefore, the leading edge of the blade is assigned to a higher power; the pressure from the leading edge to the trailing edge of the blade gradually decreases. In addition, the high-pressure area and low-pressure area appeared at the position of the blade tip and edge.

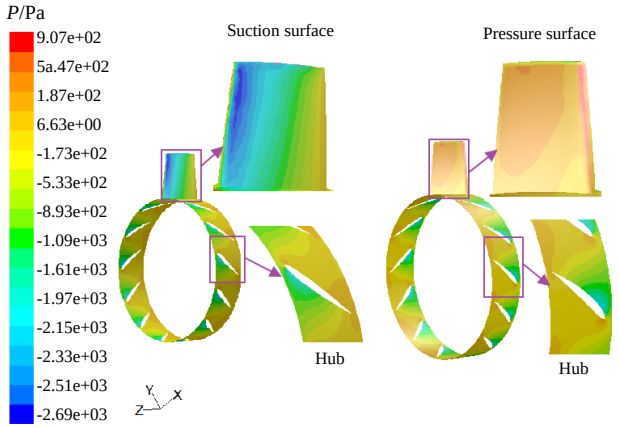

(a) The first stage impeller

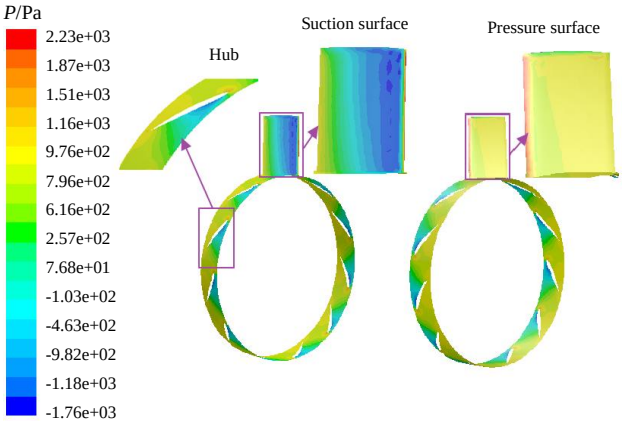

(b) The second stage impeller

Figure 5. The static pressure distribution in two-level impellers' root segments and blades

Figure 6 shows static pressure cloud map at the two impeller tips. The figure shows the static pressure in pressure surface is higher than that in suction surface, so that there is a certain adverse pressure gradient on the top of blades. It affects the normal flow of air, and it is easy to form a secondary flow loss.

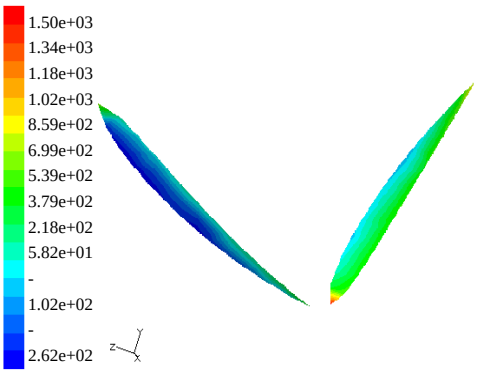

Figure 6. Static pressure cloud map at the two impeller tips

Figure 7 shows velocity vector in an axial cross; Figure 8 shows velocity cloud map in an axial section. The two following figures show that the air speed in collector and fairing is low, the air speed in the first stage motor section increases by fairing's accelerating effect, in the two impellers the speed rises to the highest, and the speed rate declines slightly in the second stage motor, while the air speed rate reduces after flowing through the diffuser. As can be seen from the Figure 7, the air flow's complete trajectory along the axis direction in the internal of the counter-rotating fan is clear; in high velocity areas the vector distribution is denser. As can be seen from Figure 8, the fluid velocity near the wall is very small, approaching to zero.

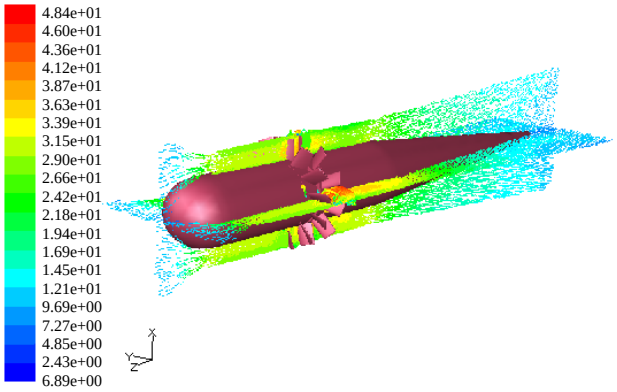

Figure 7. Velocity vector in an axial cross

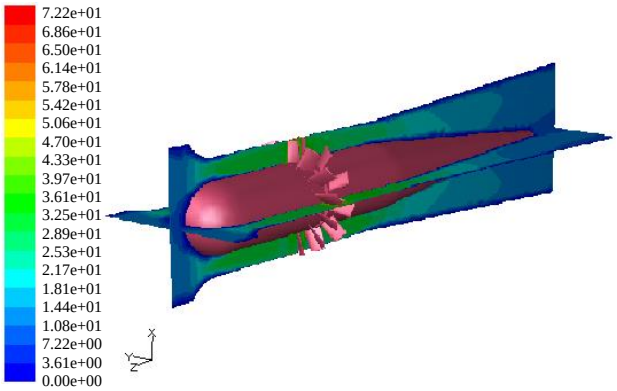

Figure 8. Velocity cloud map in an axial section

Figure 9 shows fluid trajectories in different working conditions. The flow lines are relatively stable in condition 1, the air flows regularly from the inlet to the outlet, it hardly has turbulence within the first and second flow channel, flow loss is small. When the flow is reduced to working condition 2, since the flow is less than the design flow at this time, the fan operates in an unstable state; the airflow's velocity in the first impeller's exit can't meet the requirement of airflow's velocity in the second impeller's inlet, so that the axial velocity component in the inlet of the second impeller decreases, the angle of attack increases. There is a certain angle between the outlet gas flow direction and the axial direction, and it generates obvious turbulence. Flow loss becomes large, flow lines are irregular.

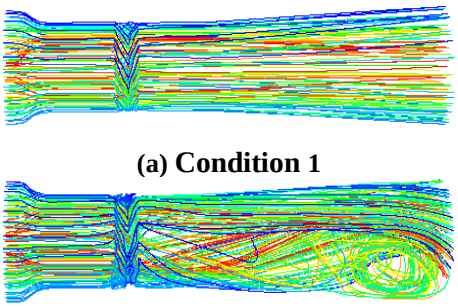

(a) Condition 1

(b) Condition 2

Figure 9. Fluid trajectories in different working conditions

4.2. Performance analysis

Figure 10 shows a wind pipe test device for the counter-rotating fan's performance test, the device is a C1-C type, the piping is the inlet side, pressure is measured in wind pipe, and the length of the inlet measurement region is 5.5m [13].

Figure 10. The wind pipe test device

Figure 11 shows the counter-rotating fan's P-Q curves in setting angle of 43 ° and 29 ° (rated speed). Where the curve 1 is obtained from tests and the curve 2 is obtained from numerical simulation. By comparing the curves 1 and 2 we can know the numerical results and experimental results are relatively close in value, and they have the same trend. This explains that the numerical results can accurately reflect the real situation of fluid flow, when the numerical simulation method is used to study the counter-rotating fan's performance, it has higher accuracy. From the curve 2, we can see that when the gas flow rate decreases, the pressure increases gradually. This is because when the counter-rotating fan operates in a stable condition zone, with the longer ventilation distance, the air resistance of the ventilation system will increase.

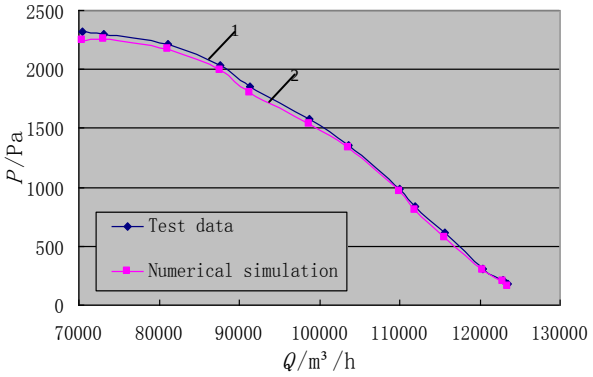

Figure 11. The P-Q curves of test data and numerical simulation data

Figure 12 shows the counter-rotating fan's P-Q curves in different blade setting angles. Curve 1 shows the static pressure characteristics curve like the shape of the saddle. When the operating point reaches the left of point B which is the highest point of the curve, the outlet pressure and the air volume lose correspondence, and the fan becomes unstable, it will lead to the counter-rotating fan's surge phenomenon and reduce equipment operation safety. Meanwhile, considering the grid voltage fluctuation may cause the speed decrease, thus we require the pressure in the operating point must not exceed the 90% of the maximum static pressure [14-15].

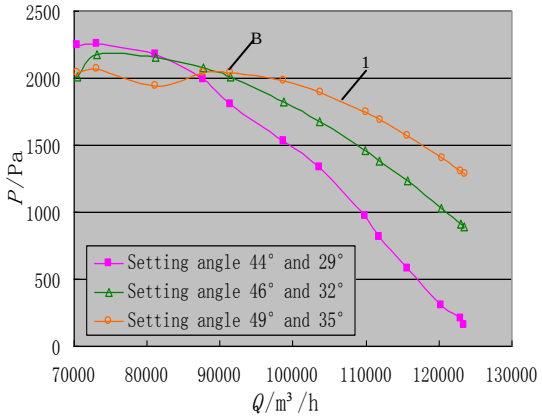

Figure 12. The counter-rotating fan's P-Q curves in different blade setting angles

In addition, the Figure 12 also shows that the counter-rotating fan's stable operating zones are different in different setting angles. With blade setting angle increases, the P-Q curves gradually move to the right, the flow rate value corresponding with the stable working condition increases gradually.

Figure 13 shows the counter-rotating fan's efficiency curves in different blade setting angles. Where the curve 1 is obtained from tests in setting angle of 43 ° and 29 °, and curves 2, 3, 4 are respectively obtained from numerical simulation in setting angles of 43 ° and 29 °,46 ° and 32 °, 49 ° and 35 °. The change trend of curve 1 and 2 is the same, the error is acceptable. In addition, the figure shows when the blade setting angle is 43 ° and 29 °, the fluctuation of efficiency is relatively large. Flow ranges which are corresponding to the high

efficiency are different under different setting angles. So when the coal mining distance increases, the counter-rotating fan's air distances increase, too. We can consider changing blade setting angles to ensure that the counter-rotating fan works in the state of the efficient operation.

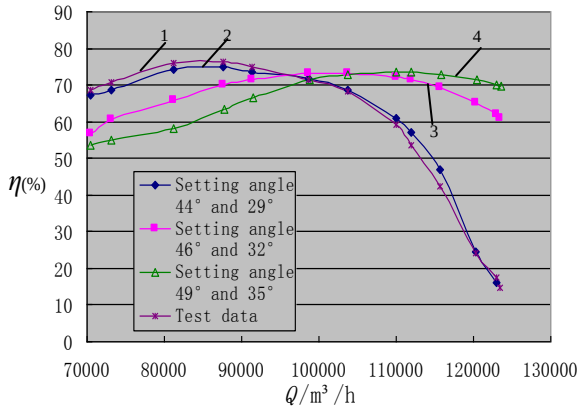

Figure 13. The counter-rotating fan's efficiency curve in different blade setting angles

5. Conclusion

In this paper, we analyze the counter-rotating fan's pressure characteristics and efficiency characteristics under different setting angles, and get distributions of pressure field and velocity field in various parts of the fan, at the same time, analyze the reason of the internal fluid disturbance. The error between numerical results with experimental data is very small within an acceptable range; it indicates that the basic assumptions and the given boundary conditions are relatively reasonable. The numerical results reveal the setting angle adjustment significantly affect on the fan's pressure and efficiency, this method can be used to predict the performance of the counter-rotating fan, optimal design and fan selection.

Acknowledgements

This project is supported by National Natural Science Foundation of China (51275137).

References

[1] C. Tan, H. Chen and X. Liang, "Three-dimensional optimization design of hundred-percent reversible subway fan", Journal of Mechanical Engineering, vol. 42, no. 9, **(2006)**, pp. 169-173.
[2] W. Zhenyu, "Problems in design of counter rotating axial fan", Compressor Blower & Fan Technology, no. 6, **(1999)**, pp. 15-17.
[3] L. Cho, H. Choi and S. Lee, "Numerical and experimental analyses for the aerodynamic design of high performance counter-rotating axial flow fans", ASME, **(2009)**.
[4] T. Shigemitsu, J. Fukutomi and Y. Okabe, "Performance and flow condition of small-sized axial fan and adoption of contra-rotating rotors", Journal of Thermal Science, vol. 19, no. 1, **(2010)**, pp. 1-6.
[5] J. -h. Zhou and C. -x. Yang, "Parametric Design and Numerical Simulation of the Axial-Flow Fan for Electronic evices", IEEE Transactions on Components and Packaging Technologies, vol. 33, no. 2, **(2010)**, pp. 287-298.
[6] L. Weili, Y. Xuefeng and G. Debao, "Calculation and Analysis of Fluid Flow and Heat Transfer of Air-Cooled Turbo-Generator With Multipath Ventilation", Transactions of China Electrotechnical Society, vol. 24, no. 12, **(2009)**, pp. 24-31.

[7] K. S. Lee, K. Y. Kim and A. Samad, "Design optimization of low-speed axial flow fan blade with three-dimensional RANS analysis", Journal of mechanical science and technology, vol. 22, no. 10, **(2008)**, pp. 1864-1869.
[8] Y. Li, H. Ouyang and Z. Du, "Experimental research on aerodynamic performance and exit flow field of low pressure axial flow fan with circumferential skewed blades", Journal of Hydrodynamics Ser. B, vol. 19, no. 5, **(2007)**, pp. 579-586.
[9] O. Yanghua, T. Jie and W. Yadong, "Aerodynamic and aeroacoustic study of collateral axial flow fan system inside outdoor unti of air-conditioner", Journal of Mechanical Engineering, vol. 43, no. 10, **(2007)**, pp. 215-220.
[10] W. Fujun, "Computational fluid dynamics analysis -CFD principle and application", Beijing: Tsinghua University Press, **(2004)**.
[11] Y. Xiao-kang, W. Li-jun, Z. Jing-song and W. Xin-yong, "Numerical and experimental investigation on effect of installation angle of rotor blade on axial flow fan", Mechanical and Electrical Technology (ICMET), **(2010)**, pp. 359-363.
[12] Z. Feng, X. Bin, L. Weili and C. Shukang, "Numerical calculation of 3d stator fluid field for large electrical machine as well as influences on thermal field distribution", Proceedings of the CSEE, vol. 25, no. 24, **(2005)**, pp. 128-132.
[13] S. Ling, "CFD analyze of flow field and test research of test-bed on blower", Urumqi: Xinjiang Agricultural University, **(2005)**.
[14] Y. H. Shin, K. H. Kim and C. S. Kang, "Unsteady pressure measurements around rotor of an axial flow fan under stable and unstable operating conditions", JSME International Journal Series B, vol. 48, no. 1, **(2005)**, pp. 56-64.
[15] J. Vad and F. Bencze, "Three-dimensional flow in axial flow fans of non-free vortex design", International journal of heat and fluid flow", vol. 19, no. 6, **(1998)**, pp. 601-607.